Chinese Physics C Vol. 50, No. 2 (2026) 024108

Nuclear matter properties from chiral-scale effective theory including a dilatonic scalar meson*

Lu-Qi Zhang (张璐琦)[1,2,3] Yao Ma (马垚)[2,3†] Yong-Liang Ma (马永亮)[2,4‡]

[1]School of Physics, Nanjing University, Nanjing 210093, China
[2]School of Frontier Sciences, Nanjing University, Suzhou 215163, China
[3]School of Fundamental Physics and Mathematical Sciences, Hangzhou Institute for Advanced Study, UCAS, Hangzhou 310024, China
[4]International Center for Theoretical Physics Asia-Pacific (ICTP-AP), UCAS, Beijing 100190, China

Abstract: Chiral effective theory has become a powerful tool for studying the low-energy properties of QCD. In this study, we apply an extended chiral effective theory—chiral-scale effective theory—including a dilatonic scalar meson to study nuclear matter. It is found that the properties around saturation density can be well reproduced. Compared to Walecka-type models in nuclear matter studies, our approach improves the behavior of symmetry energy in describing empirical data without introducing an additional isovector scalar meson δ to make it soft at intermediate densities. Moreover, the predicted neutron star mass-radius relations fall within the constraints of GW170817, PSR J0740+6620, and PSR J0030+0451, while the maximum neutron star mass can reach $\gtrsim 2.5M_{\odot}$ with a pure hadronic phase. Additionally, we find that symmetry patterns of the effective theory significantly impact neutron star structures. We believe that introducing this type of theory into nuclear matter studies can contribute to a more comprehensive understanding of QCD, nuclear matter, and compact astrophysical objects.

Keywords: nuclear matter, neutron star, scale symmetry, chiral effective theory

DOI: 10.1088/1674-1137/ae18ae **CSTR:** 32044.14.ChinesePhysicsC.50024108

I. INTRODUCTION

The study of nuclear matter (NM) has long been crucial for understanding both nuclear force and neutron star (NS) mass-radius (M-R) relations (see, *e.g.*, Refs. [1−7] and references therein). The properties of NM are highly sensitive to the specifics of nucleon interactions. A popular and widely used approach to describe these interactions is the one-boson-exchange (OBE) model and its variants, such as the Walecka-type models [8−11]. These models typically involve π, σ, ω, and ρ meson exchanges, covering the effective range of nucleon forces from 0.5 to 2 fm. Utilizing these models, NM properties can be calculated using the relativistic mean field (RMF) approach [12−15], which is the most practical and economical framework to introduce density effects.

It is recognized that Walecka-type models lack the consideration of QCD symmetry patterns, the valid region of effective operators, and theoretical errors. While chiral effective field theory (χEFT), thanks to the pioneering works by Weinberg [16, 17], offers a powerful framework for studying nuclear forces at long ranges, it is anchored on QCD symmetry by treating the pion as the Nambu-Goldstone (NG) boson of spontaneous chiral symmetry breaking. Due to the derivative couplings [18, 19], operators can be organized systematically according to the chiral expansion by q/Λ, where q is the momentum scale carried by the NG bosons and $\Lambda = 4\pi f_\pi \sim 1$ GeV is the scale of chiral symmetry breaking. The valid region and theoretical errors of χEFT can be determined by estimating the truncation of the chiral expansion [20−22].

To develop a realistic model of nuclear forces, it is accepted that vector mesons—ρ and ω— and the isoscalar-scalar meson σ are indispensable. However, the original χ EFT, which only contains NG modes, will encounter divergence due to the emergence of σ, ρ, and ω mesons [23, 24]. To avoid this and extend the valid region of effective operators, hidden local symmetry (HLS) in χEFT [25−27] plays a crucial role by including the vector mesons. However, the inclusion of the σ meson as an independent degree of freedom in χEFT is not straightfor-

Received 4 June 2025; Accepted 27 October 2025; Accepted manuscript online 28 October 2025

* The work of Y. M. is supported by by Jiangsu Funding Program for Excellent Postdoctoral Talent under Grant Number 2025ZB516. Y. L. M. is supported in part by the National Science Foundation of China (NSFC) under Grant No. 12347103, the National Key R&D Program of China under Grant No. 2021YFC2202900 and Gusu Talent Innovation Program under Grant No. ZXL2024363..

† E-mail: mayao@nju.edu.cn
‡ E-mail: ylma@nju.edu.cn

ward, as the fourth scalar component of the chiral four-vector is integrated out when transitioning from the linear to nonlinear sigma model—the leading term of χEFT. Considering that the lowest-lying scalar meson σ has approximately equivalent mass to that of the kaon, which is an NG boson of chiral symmetry breaking in three-flavor χEFT ($\chi\mathrm{EFT}_3$), by supposing that QCD has a nonperturbative infrared fixed point, Crewther and Tunstall [28, 29] proposed that the lowest-lying scalar meson can be considered as the NG boson (dilaton) of the spontaneous breaking of scale symmetry. Consequently, χEFT was extended to include the scalar meson, resulting in the scale-chiral effective theory ($\chi\mathrm{EFT}_\sigma$). This approach is different from the Walecka-type models, which add these hadron resonances and corresponding interactions by the necessity of the phenomenological analysis, without considering the symmetry argument and power counting.

Based on the terminologies of $\chi\mathrm{EFT}_\sigma$ and HLS, χEFT with baryons was constructed in Refs. [30, 31] at the leading chiral order to discuss nucleon interactions; it is denoted as bsHLS, where "b" and "s" represent baryon and scale, respectively. In bsHLS, the potential from meson exchanges in OBE models can be reproduced by expanding to the first order of linear field couplings but with additional symmetry considerations. By using the low-momentum potential $V_{\rm lowk}$ renormalization group approach [32, 33], taking the "leading order scale symmetry (LOSS)" approximation, where the trace anomaly effect enters only through the dilaton potential, which breaks scale symmetry explicitly and spontaneously, we found that the chiral-scale EFT with few parameters can successfully describe not only NM at the saturation density but also compact-star matter at $n=(5-7)n_0$ [6]. A novel phenomena that was not realized before is that in nuclear matter at densities $n=(2-4)n_0$, the sound velocity of NM may saturate the conformal limit $v_s^2=1/3$, but the trace of the energy-momentum tensor does not vanish, that is, NM exhibits a pseudo-conformal structure [34−36]. Moreover, corrections to LOSS in the baryonic part have been crucial for understanding the quenched g_A value in the super-allowed Gamow-Teller transitions of heavy nuclei [37, 38].

In this study, we investigate NM properties using bsHLS with the RMF method. After identifying the NM properties around n_0, it was found that bsHLS using the RMF method can yield reasonable results. The data can be reproduced with the choice of $\beta'=\frac{\partial\beta}{\partial\alpha}\sim 1$, consistent with the results of Refs. [39, 40], where a fixed dilaton limit point is assumed in the medium. The combination of $f_\chi m_\sigma$ is constrained to $\simeq 2.3\times10^5$ MeV^2, which is consistent with existing estimations via the skyrmion crystal approach, such that physically interesting results can be obtained [41, 42]. By comparing the symmetry energy $E_{\rm sym}$ and incompressibility coefficient $K(n)$ obtained from our bsHLS and Walecka-type models, we find that bsHLS can make the symmetry energy stiff at subsaturation density but soft at intermediate densities to meet the constraints of GW170817 [43] and the neutron skin thickness of ^{208}Pb [44] simultaneously, without introducing additional freedoms, such as the δ meson in Refs. [45, 46]. In addition, we find that the incompressibility coefficient of bsHLS surges at intermediate densities, while the Walecka-type models exhibit gentler behaviors, resulting in a better description of the NS M-R relation using bsHLS. The maximum mass of NS can almost reach $3M_\odot$ with a pure hadron phase, meeting the constraints of GW170817 [43, 47] and PSR J0740+6620 [48, 49], whereas the Walecka-type models compared in this work, which saturate these constraints, yield a maximum mass of approximately $2.2M_\odot$ [50−52]. This is due to the kink behavior of σ expectations at intermediate densities, induced by the nonlinear realization of scale symmetry. Moreover, the value of β', behavior of $\langle\chi\rangle^*$, and Brown-Rho (B-R) scaling at different densities can significantly affect NS M-R relations, indicating a relationship between QCD symmetry patterns and macroscopic phenomena.

The remainder of this article is organized as follows: In Sec. II, we introduce the theoretical framework of bsHLS and the equation of state (EoS) of NM under the RMF approximation. In Sec. III, we provide a phenomenological analysis based on experimental data of nuclear matter and neutron star observations. A comparison with the Walecka-type models is also made. Finally, a summary and discussion are presented in Sec. IV.

II. BSHLS IN NUCLEAR MEDIUM

In this section, we establish the theoretical framework of bsHLS and derive the EoS for NM within the RMF approach. Focusing on NM only composed of nucleons, we restrict the bsHLS Lagrangian to the two-flavor case, involving only u and d quarks. The leading order bsHLS Lagrangian $\mathcal{L}$ can be decomposed into the baryonic part $\mathcal{L}_B$ and mesonic part $\mathcal{L}_M$:

$$\mathcal{L}=\mathcal{L}_M+\mathcal{L}_B\,. \tag{1}$$

The mesonic part $\mathcal{L}_M$, consisting of σ, ρ, ω, and π mesons, is constructed as follows [31]:

$$\begin{aligned}\mathcal{L}_M={}&f_\pi^2\Phi^2\left[h_1+(1-h_1)\Phi^{\beta'}\right]\mathrm{Tr}\left(\hat{\alpha}_\perp^\mu\hat{\alpha}_{\mu\perp}\right)\\&+\frac{m_\rho^2}{g_\rho^2}\Phi^2\left[h_2+(1-h_2)\Phi^{\beta'}\right]\mathrm{Tr}\left(\hat{\alpha}_\parallel^\mu\hat{\alpha}_{\mu\parallel}\right)\\&+\frac{1}{2}\left(\frac{m_\omega^2}{g_\omega^2}-\frac{m_\rho^2}{g_\rho^2}\right)\Phi^2\left[h_3+(1-h_3)\Phi^{\beta'}\right]\end{aligned}$$

$$
\begin{aligned}
&\times \mathrm{Tr}\left(\hat{\alpha}_{\|}^{\mu}\right)\mathrm{Tr}\left(\hat{\alpha}_{\mu\|}\right)+\frac{1}{2}\left[h_4+(1-h_4)\Phi^{\beta'}\right]\partial_\mu\chi\partial^\mu\chi \\
&+\frac{f_\pi^2}{4}\Phi^{3-\gamma_m}\mathrm{Tr}\left(\mathcal{M}U^\dagger+U\mathcal{M}^\dagger\right)+h_5\Phi^4+h_6\Phi^{4+\beta'} \\
&-\frac{1}{2g_\rho^2}\left[h_7+(1-h_7)\Phi^{\beta'}\right]\mathrm{Tr}\left(V_{\mu\nu}V^{\mu\nu}\right) \\
&-\frac{1}{2g_0^2}\left[h_8+(1-h_8)\Phi^{\beta'}\right]\mathrm{Tr}\left(V_{\mu\nu}\right)\mathrm{Tr}(V^{\mu\nu})\ ,
\end{aligned} \tag{2}
$$

where $V_{\mu\nu}=\partial_\mu V_\nu-\partial_\nu V_\mu-\mathrm{i}\left[V_\mu,V_\nu\right]$ and $V_\mu=\frac{1}{2}(g_\omega\omega_\mu+g_\rho\rho_\mu^a\tau^a)$. m_ρ, m_ω, and $\mathcal{M}=m_\pi^2 I_{2\times2}$ are the masses of ρ, ω, and π mesons, respectively. The dilaton field χ is introduced as a nonlinear representation $\chi=f_\chi\Phi=f_\chi\exp\left(\sigma/f_\chi\right)$, and β' accounts for the anomalous dimension of gluon field operators, representing the deviation from the IR fixed point. According to Ref. [53], the h_is, except h_5 and h_6, are chosen to be 1 for simplification, and the anomalous dimension γ_m is also simply taken to be 1 (denoted as LOSS). h_5 and h_6 are constrained by the saddle point equations

$$
\begin{aligned}
&4h_5+(4+\beta')h_6+2m_\pi^2 f_\pi^2=0\ , \\
&12h_5+(4+\beta')(3+\beta')h_6+2m_\pi^2 f_\pi^2=-m_\sigma^2 f_\chi^2\ .
\end{aligned} \tag{3}
$$

In Lagrangian (2), pions are introduced as a nonlinear field $\xi=\sqrt{U}=\mathrm{e}^{\mathrm{i}\frac{\pi}{f_\pi}}$, where $\pi=\pi^a\frac{\tau^a}{2}$, with $a=1,2,3$ representing the isospin indices. Its covariant derivative is defined as

$$
D_\mu\xi=\left(\partial_\mu-\mathrm{i}V_\mu\right)\xi=\left[\partial_\mu-\mathrm{i}\frac{1}{2}\left(g_\omega\omega_\mu+g_\rho\rho_\mu^a\tau^a\right)\right]\xi\ . \tag{4}
$$

The Murrer-Cartan 1-forms $\hat{\alpha}_\perp^\mu$ and $\hat{\alpha}_\|^\mu$ are defined as

$$
\hat{\alpha}_{\perp,\|}^\mu=\frac{1}{2\mathrm{i}}\left(D^\mu\xi\cdot\xi^\dagger\mp D^\mu\xi^\dagger\cdot\xi\right)\ . \tag{5}
$$

The baryonic part of the Lagrangian $\mathcal{L}_B$ is written as [31]

$$
\begin{aligned}
\mathcal{L}_B=&\left[g_1+(1-g_1)\Phi^{\beta'}\right]\bar{N}\mathrm{i}\gamma_\mu D^\mu N \\
&-\left[g_2+(1-g_2)\Phi^{\beta'}\right]m_N\Phi\bar{N}N \\
&+\left[g_A C_A+g_A(1-C_A)\Phi^{\beta'}\right]\bar{N}\hat{\alpha}_\perp^\mu\gamma_\mu\gamma_5 N \\
&+\left[g_{V_\rho}C_{V_\rho}+g_{V_\rho}\left(1-C_{V_\rho}\right)\Phi^{\beta'}\right]\bar{N}\hat{\alpha}_\|^\mu\gamma_\mu N \\
&+\frac{1}{2}\left[g_{V_0}C_{V_0}+g_{V_0}\left(1-C_{V_0}\right)\Phi^{\beta'}\right]\mathrm{Tr}\left[\hat{\alpha}_\|^\mu\right]\bar{N}\gamma_\mu N\ ,
\end{aligned} \tag{6}
$$

where N is the iso-doublet of baryon field, and g_1 and g_2 are set to 1 as suggested in Ref. [53]. For convenience, we introduce the following combinations of the parameters:

$$
\begin{aligned}
g_{\omega NN}&=\frac{1}{2}\left(g_{V_\rho}C_{V_\rho}+g_{V_0}C_{V_0}-1\right)g_\omega\ , \\
g_{\rho NN}&=\frac{1}{2}\left(g_{V_\rho}C_{V_\rho}-1\right)g_\rho\ , \\
g_{\omega NN}^{SSB}&=\frac{1}{2}\left[g_{V_\rho}\left(1-C_{V_\rho}\right)+g_{V_0}\left(1-C_{V_0}\right)\right]g_\omega\ , \\
g_{\rho NN}^{SSB}&=\frac{1}{2}\left[g_{V_\rho}\left(1-C_{V_\rho}\right)\right]g_\rho\ .
\end{aligned} \tag{7}
$$

By regarding the NM as homogeneous matter, the RMF approximation can be applied. Using Lagrangian (1), the EOMs of ω and ρ can be obtained as

$$
\begin{aligned}
&m_\omega^2\Phi^2\omega-\left[g_{\omega NN}+g_{\omega NN}^{SSB}\left(\Phi^{\beta'}-1\right)\right]\left(\rho_n+\rho_p\right)=0\ , \\
&m_\rho^2\Phi^2\rho-\left[g_{\rho NN}+g_{\rho NN}^{SSB}\left(\Phi^{\beta'}-1\right)\right]\left(\rho_p-\rho_n\right)=0\ ,
\end{aligned} \tag{8}
$$

where ρ and ω denote fields for brevity. Similarly, the EOM of the σ field is derived as

$$
\begin{aligned}
m_\omega^2\omega^2\Phi+m_\rho^2\rho^2\Phi=&\frac{m_N^4\Phi^3}{\pi^2}\left[F\left(\frac{k_p}{m_N\Phi}\right)+F\left(\frac{k_n}{m_N\Phi}\right)\right] \\
&-2f_\pi^2 m_\pi^2\Phi-4h_5\Phi^3-(4+\beta')h_6\Phi^{3+\beta'} \\
&+g_{\omega NN}^{SSB}\beta'\Phi^{\beta'-1}\omega\left(\rho_p+\rho_n\right) \\
&+g_{\rho NN}^{SSB}\beta'\Phi^{\beta'-1}\rho\left(\rho_p-\rho_n\right)\ ,
\end{aligned} \tag{9}
$$

where $\frac{m_N^3\Phi^3}{\pi^2}F\left(\frac{k_{p(n)}}{m_N\Phi}\right)$ refers to scalar density $\langle\bar{p}p\rangle$ or $\langle\bar{n}n\rangle$, and $k_{p(n)}$ is the Fermi momentum of nucleons at zero temperature.

The energy density can be obtained via Lagrangian (1) with the solutions of EOMs given above:

$$
\begin{aligned}
\langle\mathcal{H}\rangle=&-\mathrm{i}\langle\bar{N}\gamma_i\partial^i N\rangle+m_N\Phi\langle\bar{N}N\rangle+\frac{1}{2}m_\omega^2\Phi^2\omega^2 \\
&+\frac{1}{2}m_\rho^2\Phi^2\rho^2-f_\pi^2 m_\pi^2\Phi^2-h_5\Phi^4-h_6\Phi^{4+\beta'} \\
=&\frac{m_N^4\Phi^4}{\pi^2}\left[f\left(\frac{k_p}{m_N\Phi}\right)+f\left(\frac{k_n}{m_N\Phi}\right)\right] \\
&+\frac{1}{2}m_\omega^2\Phi^2\omega^2+\frac{1}{2}m_\rho^2\Phi^2\rho^2 \\
&-f_\pi^2 m_\pi^2\Phi^2-h_5\Phi^4-h_6\Phi^{4+\beta'}\ ,
\end{aligned} \tag{10}
$$

where $f\left(\frac{k_p(n)}{m_N\Phi}\right)=\int_0^{\frac{k_{p(n)}}{m_N}}x'^2\sqrt{1+x'^2}\mathrm{d}x'$. It should be noted that the nonlinear Lagrangian (1) will lead to nonzero constant vacuum energy $\mathcal{E}_0=-f_\pi^2 m_\pi^2-h_5-h_6$, which is neglected in our EOS calculations.

The above bsHLS (1) is constructed in a matter-free space. When applying it to a medium, it is natural to expect that the parameters in the Lagrangian should be changed by medium, *i.e.*, density in this case. We implement this density effect via B-R scaling [2, 54] and refer to this density effect as intrinsic density dependence (IDD). Explicitly, the parameters in Lagrangian (1) scale as

$$\frac{m^*_{\rho(\omega,N)}}{m_{\rho(\omega,N)}} \approx \frac{f^*_\pi}{f_\pi} \approx \Phi^* , \quad \frac{m^*_\sigma}{m_\sigma} \approx (\Phi^*)^{1+\frac{\beta'}{2}} . \tag{11}$$

A possible choice of Φ^* is $1/(1+r\frac{\rho_n+\rho_p}{n_0})$. Pion-nuclei bound state data [55] indicate $r \approx 0.2$, but we set it as a free parameter to fit the NM properties in this work. Chiral dynamics indicate that pion mass is not changed by medium, so we set $m^*_\pi/m_\pi \approx 1$. The saddle point equation (3) leads to

$$h^*_5 = \frac{-2(2+\beta')m^{*2}_\pi f^{*2}_\pi + m^{*2}_\sigma f^{*2}_\chi}{4\beta'} , \quad h^*_6 = \frac{4m^{*2}_\pi f^{*2}_\pi - m^{*2}_\sigma f^{*2}_\chi}{(4+\beta')\beta'} . \tag{12}$$

After the above discussions, we finally obtain the energy density for phenomenological analysis as

$$\begin{aligned}\mathcal{E} = {} & \frac{m^{*4}_N \Phi^4}{\pi^2}\left[f\left(\frac{k_p}{m^*_N\Phi}\right) + f\left(\frac{k_p}{m^*_N\Phi}\right)\right] \\ & + \frac{1}{2}m^{*2}_\omega \Phi^2 \omega^2 + \frac{1}{2}m^{*2}_\rho \Phi^2 \rho^2 \\ & - f^{*2}_\pi m^2_\pi \Phi^2 - h^*_5 \Phi^4 - h^*_6 \Phi^{4+\beta'} - \mathcal{E}^*_0 .\end{aligned} \tag{13}$$

III. PHENOMENOLOGICAL ANALYSIS

In the phenomenological analysis, we choose vacuum values $f_\pi = 92.4$ MeV, $m_N = 939$ MeV, $m_\pi = 140$ MeV, $m_\omega = 783$ MeV, and $m_\rho = 765$ MeV [56]. The free parameters are $M_\sigma = m_\sigma f_\chi$, β', r, $g_{\omega NN}$, $g_{\rho NN}$, $g^{SSB}_{\omega NN}$, and $g^{SSB}_{\rho NN}$, which can be estimated by the properties of NM around saturation density n_0. The calculated results of NM properties are listed in Table 1, and the corresponding low energy constants (LECs) are given in Table 2. It can be seen that NM properties obtained from both bsHLS-L and bsHLS-H are consistent with empirical values.

To illustrate the features of bsHLS, we consider a Walecka-type model [65] for comparison:

$$\begin{aligned}\mathcal{L}_{\rm RMF} = {} & \bar\psi\left[i\gamma_\mu\partial^\mu - (m_N - g_\sigma\sigma - g_\delta\delta^a\tau^a)\right. \\ & \left. - g_{\omega NN}\gamma_\mu\omega^\mu - g_{\rho NN}\gamma_\mu\rho^{\mu a}\tau^a\right]\psi \\ & + \frac{1}{2}\left(\partial_\mu\sigma\partial^\mu\sigma - m^2_\sigma\sigma^2\right) - \frac{1}{3}g_2\sigma^3 \\ & - \frac{1}{4}g_3\sigma^4 - \frac{1}{4}F_{\mu\nu}F^{\mu\nu} + \frac{1}{2}m^2_\omega\omega_\mu\omega^\mu \\ & + \frac{1}{4}c_3 g^4_{\omega NN}\left(\omega_\mu\omega^\mu\right)^2 - \frac{1}{4}B^a_{\mu\nu}B^{\mu\nu a} \\ & + \frac{1}{2}m^2_\rho\rho^{\mu a}\rho^a_\mu + g_\sigma g^2_{\omega NN}\sigma\omega_\mu\omega^\mu\left(\alpha_1 + \frac{1}{2}\alpha'_1 g_\sigma\sigma\right) \\ & + g_\sigma g^2_{\rho NN}\sigma\rho^{\mu a}\rho^a_\mu\left(\alpha_2 + \frac{1}{2}\alpha'_2 g_\sigma\sigma\right) \\ & + \frac{1}{2}\alpha'_3 g^2_{\omega NN} g^2_{\rho NN}\omega_\mu\omega^\mu\rho^{\nu a}\rho^a_\nu \\ & + \frac{1}{2}\left(\partial_\mu\delta^a\partial^\mu\delta^a - m^2_\delta\delta^a\delta^a\right) + \frac{1}{2}C_{\delta\sigma}g^2_\sigma g^2_\delta\sigma^2\delta^a\delta^a .\end{aligned} \tag{14}$$

Table 1. Properties of nuclear matter: e_0 is the binding energy of nucleon at n_0, $E_{\rm sym}(n) = \frac{1}{2}\frac{\partial^2 E(n,\alpha)}{\partial\alpha^2}\Big|_{\alpha=0}$ is the symmetry energy, $K_0 = 9n^2\frac{\partial^2 E(n,0)}{\partial n^2}\Big|_{n=n_0}$ is the incompressibility coefficient, $J_0 = 27n^3\frac{\partial^3 E(n,0)}{\partial n^3}\Big|_{n=n_0}$ is the skewness coefficient, and $L(n) = 3n\frac{\partial E_{\rm sym}(n)}{\partial n}$ is the symmetry energy density slope. $n_c \approx 0.11{\rm fm}^{-3}$ is subsaturation cross density. Two sets of predictions are shown: bsHLS-L refers to the case where the surge of $K(n)$ is located at lower density regions, and bsHLS-H refers to the higher density case. n_0 is in units of ${\rm fm}^{-3}$, and the others are in units of MeV.

	Empirical	bsHLS-L	bsHLS-H
n_0	0.155 ± 0.050 [57]	0.159	0.159
e_0	-15.0 ± 1.0 [57]	−16.0	−16.0
K_0	230 ± 30 [58]	232	284
$E_{\rm sym}(n_c)$	22.4 ± 2.3 [59, 60]	20.8	20.9
$E_{\rm sym}(n_0)$	30.9 ± 1.9 [61]	30.5	29.2
$E_{\rm sym}(2n_0)$	46.9 ± 10.1 [62]	51.5	50.2
$L(n_c)$	43.7 ± 7.8 [63]	53.2	54.2
$L(n_0)$	52.5 ± 17.5 [57, 61]	85.9	68.3
J_0	-400 ± 390 [64]	−767	−599

The choices of parameters from some references are listed in Table 3.

A. Nuclear matter properties

The properties of NM are analyzed first. From Table 1, one can see that, with appropriate choices of parameters in Table 2, our bsHLS can yield NM properties around (sub)saturation density, satisfying the constraints from empirical data.

Regarding the $L(n_c)$ results listed in Table 1, both bsHLS-L and bsHLS-H exhibit the stiffness to align with the neutron skin thickness of $\rm Pb^{208}$ [44], as well as the Walecka-type models compared in this work, as shown in Fig. 1. Moreover, the $E_{\rm sym}$ behavior of bsHLS is similar to that of the compared Walecka-type models at low densities $n \lesssim n_0$. However, at intermediate densities around $2n_0$, the models can be categorized into three sets: bsHLS and FSU-δ6.7 yield the most soft $E_{\rm sym}$, whereas

Table 2. Estimation of parameters for bsHLS-L and bsHLS-H.

	$M_\sigma/(10^5\text{MeV}^2)$	β'	r	$g_{\omega NN}$	$g_{\rho NN}$	$g^{SSB}_{\omega NN}$	$g^{SSB}_{\rho NN}$
bsHLS-L	1.05	0.395	0.161	11.5	3.78	16.3	9.45
bsHLS-H	2.30	1.15	0.191	11.0	4.17	8.85	4.85

Table 3. Choice of parameters for Walekca-type models in Eq. (14).

	NL3[66]	TM1[67]	FSU-δ6.7[45]	BKA22[68]	BSR12[69]
n_0/fm^{-3}	0.148	0.145	0.148	0.147	0.147
m_N/MeV	939	938	938	939	939
m_σ/MeV	508	511	492	498	499
m_ω/MeV	783	783	783	782	783
m_ρ/MeV	763	770	763	770	763
m_δ/MeV	0	0	980	0	0
g_σ	10.2	10.0	10.2	10.6	10.6
$g_{\omega NN}$	12.9	12.6	13.4	13.9	13.9
$g_{\rho NN}$	4.47	4.63	7.27	6.47	5.48
g_δ	0	0	6.70	0	0
g_2/fm^{-1}	10.4	7.23	8.09	11.0	10.6
g_3	-28.9	0.618	5.88	11.3	10.2259
$c_3(10^{-3})$	0	2.82	5.28	5.00	5.00
$\alpha_1/(\text{fm}^{-1}\cdot 10^{-3})$	0	0	0	1.32	1.26
$\alpha'_1(10^{-3})$	0	0	0	0.124	0.00520
α_2/fm^{-1}	0	0	0	0.150	0.0475
$\alpha'_2(10^{-2})$	0	0	0	0	5.10
$\alpha'_3(10^{-2})$	0	0	2.14	0	1.16
$C_{\delta\sigma}(10^{-2})$	0	0	3.85	0	0

NL3 and TM1 give most stiff one, and BSR12 and BKA22 fall in between. The Walecka-type models without the δ meson are not soft sufficient at the intermediate densities, while bsHLS provides a more reasonable behavior without introducing δ.

It will be seen later that this difference can affect the tidal deformation of NS.

For the incompressibility, the results of bsHLS and the compared Walekca-type models show significant differences at intermediate densities: Walecka-type models exhibit a monotonic behavior with density, whereas bsHLS shows a kink behavior around $(1\sim 2)n_0$. This kink behavior results in a peak structure in the sound velocity, which plays an important role in determining the M-R relation of NS and is attributed to the manifestation of scale symmetry in nuclear matter [70].

B. Neutron star structures

Next, the NS M-R relations are studied using the EOSs discussed above for pure neutron matter (PNM). The results of NS M-R relations are shown in Fig. 2 and Table 4

From Fig. 2, all the M-R relations satisfy the casual limits, but the parts of bsHLS and NL3 near and past the maximum mass point fall into the negative trace anomaly region. However, the trace anomaly constraint is estimated from the pQCD side, whose corresponding density region is above $(20-30)n_0$ [78], which is far from the central density of an NS core. In fact, M-R relations can be improved by correcting the scale symmetry pattern to have a physically reasonable behavior in the high density region, as discussed later in this section. Besides, one can see that the M-R relation obtained from bsHLS-L cannot satisfy the radius constraint, which will be also discussed in detail in the next section.

bsHLS-H predicts that an M-R relation falls within the constraints of astro-observations with an obviously larger maximum mass around $2.8M_\odot$, compared to Walecka-type models: when meeting the NS constraints, the

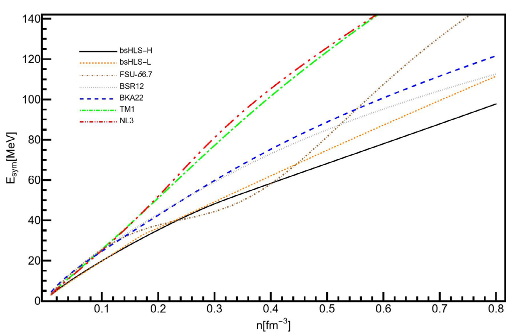

(a) Symmetry energy as a function of density.

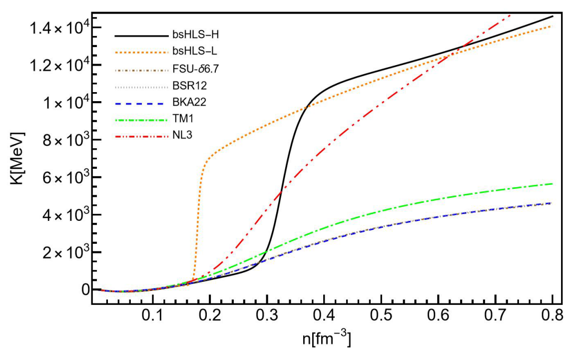

(b) Incompressibility as a function of density.

Fig. 1. (color online) Incompressibility, $K=9\frac{dP}{dn}$, which is reduced to K_0 at n_0, and symmetry energy of symmetric NM from bsHLS and Walecka-type models.

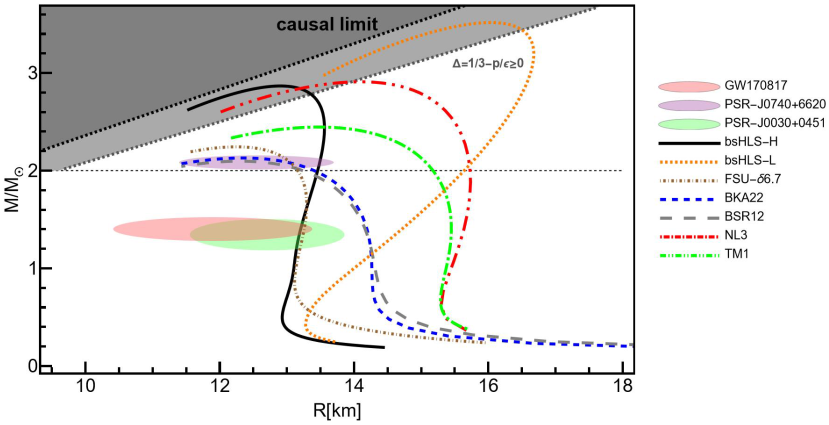

Fig. 2. (color online) M-R relations from bsHLS and Walecka-type models. The constraints are estimated from Refs. [43, 47, 49, 71, 72]. The M-R relation is calculated by solving the Tolman-Oppenheimer-Volkoff (TOV) equation [73, 74]. All EoSs for TOV equation calculation are interpolated to a BPS EoS [75] below $0.01\ \mathrm{fm}^{-3}$ [76].

Table 4. Tidal deformations from bsHLS and Walecka-type models defined in Eq. (14) and Table 3 for NS with mass of $1.4\ M_\odot$. They are calculated from the EOSs used for the M-R relation in Fig. 2, using the formalisms in Ref. [77].

	Empirical [43]	bsHLS-L	bsHLS-H	TM1	NL3	FSU-δ6.7	BKA22	BSR12
$\Lambda_{1.4}$	190^{+390}_{-120}	2120	910	2240	2826	878	1348	1245

$M_{\rm max}$ of NSs predicted by these Walecka-type models is around or slightly above $2.2M_\odot$, as discussed in Refs. [50−52, 79, 80].

Although the result from FSU-δ6.7 satisfies these constraints, it requires a new degree of freedom δ to be introduced. The Walecka-type models without δ considered in this study cannot provide consistent results with the constraints of NSs, though they reproduce the NM properties around n_0 [67, 81]. This highlights the advantage of bsHLS in interpreting the structures of nuclei and NSs within a unified framework. In addition, because of the larger predicted $M_{\rm max}$, $\sim 2.8M_\odot$, which is close to the upper limit of NS of the gap problem in the continuous mass distribution of supernova remnants [82, 83], by pure hadron matter with bsHLS-H, this new approach may have profound implications for understanding the gravitational wave event GW190814 [84].

For tidal deformations from Table 4, one can conclude that only the results of bsHLS-H and FSU-δ6.7 are close to the constraints of GW170817 [43]. This is due to the softness of $E_{\rm sym}$ from these two at intermediate densities, as shown in Fig. 1. However, the tidal deformation of bsHLS-L is very large, though the symmetry energy at intermediate densities is also soft. This is due to the very early surge of incompressibility, as shown in Fig. 1, leading to large maximum mass of NS and a more distorted M-R relation: compact NSs for small mass ones but loose NSs to reach such a large maximum mass. The same reasoning applies to the Walecka-type models, NL3, TM1, BKA22, and BSR12.

To show the rationality of the above discussions, we also plot the M-R relations in beta equilibrium matter—a more realistic case but beyond the present framework—in Fig. 3. One can see that the maximum mass of an NS does not change much, while the M-R relations all become more compact, favored by observations. Thus, the inclusion of beta equilibrium matter does not change the main conclusion drawn above.

In summary, the above discussion stresses that, in contrast to the Walecka-type models, where the isovector scalar δ is needed, the bsHLS anchored on the chiral and scale symmetries of QCD with self-consistent power counting can yield phenomenological results that align with the observation data and predict the maximum mass above $2.5M_\odot$. It also implies that the scaling parameter $r\approx 0.19$, $\beta'\approx 1.15$, $M_\sigma = m_\sigma f_\chi \approx 2.3\times 10^5\ \mathrm{MeV}^2$, and the couplings between vector mesons and nucleons $g_{\rho NN}\approx 4.17$, $g_{\omega NN}\approx 11.0$. The scaling parameter $r\approx 0.19$ is consistent with pion-nuclei bound state data [55], while $\beta'\approx 1.15$ agrees with estimates from the skyrmion crystal approach [39, 40]. If f_χ is taken to be $3f_\pi\approx 270\ \mathrm{MeV}$, $m_\sigma\approx 850\ \mathrm{MeV}$, while the power-counting mechanism of Crewther and Tuntall remains valid [28]. The coupling constant $g_{\rho NN}\approx 4.17$ aligns with the results from the OBE potential analysis of nucleon interactions [9], and $g_{\omega NN}\approx 11.0$ is in agreement with the analyses of nucleon-nucleon scatterings [85].

C. Patterns of scale symmetry and phenomenologies

The difference between bsHLS-L and bsHLS-H becomes significant in the M-R relation, as shown in Fig. 2 and discussed in the previous section, though it is not dis-

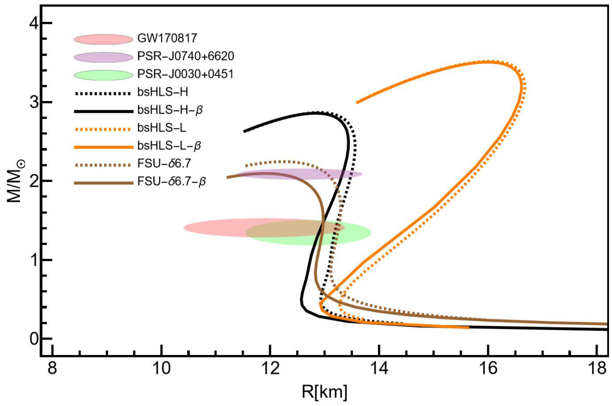

Fig. 3. (color online) M-R relations from bsHLS and Walecka-type models based on PNM and beta equilibrium matter calculations.

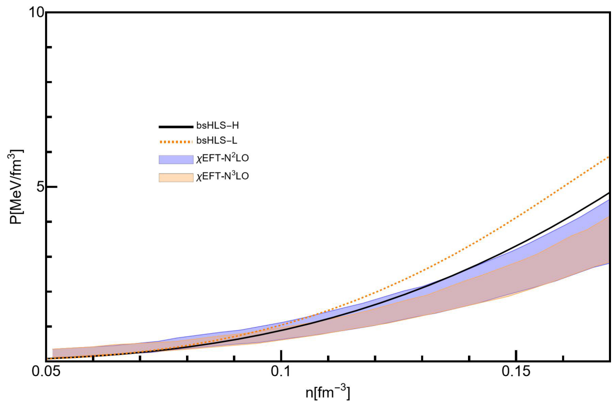

Fig. 4. (color online) Pressure as a function of density for PNM. The orange and blue shaded regions come from N^{2}LO and N^{3}LO of chiral nulear force results, respectively [86].

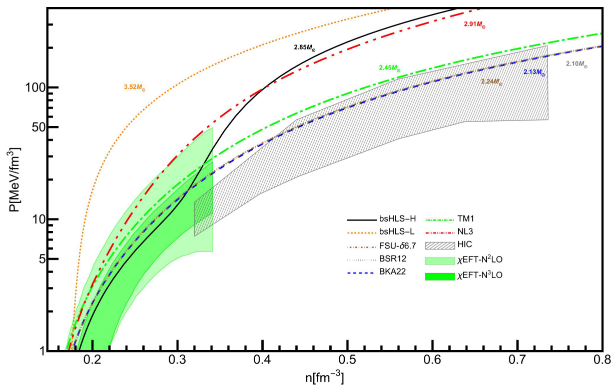

Fig. 5. (color online) Pressure as a function of density for SNM. The gray hatched area represents the constraints from Au+Au flow-data analysis [87]. The green shaded region comes from chiral nuclear force results [88]. The numbers next to the curves represent the predicted maximum masses of neutron stars.

tinguishable from the NM properties around saturation density. To understand these more deeply, the pressure of PNM is calculated around and below saturation density and compared with the results of the conventional chiral nuclear force, as shown in Fig. 4. One can see that the pressure of bsHLS-H can align with the constraints up to saturation density, while bsHLS-L is slightly higher around n_0. However, at low densities, below 0.1 fm^{-3}, the chiral nuclear force and bsHLS results are consistent with each other because the mesons can be integrated out at this region in the description of nucleon interactions, leading to the equivalence of the two approaches. This strengthens the validity of our results.

Furthermore, we plot the SNM pressure beyond the saturation density and compare it with the heavy ion collision (HIC) analysis and chiral nuclear force results in Fig. 5. It can be seen that the results of BSR12, BKA22, and FSU-δ6.7 can fall in the region above $2.5n_0$, which mostly influences the maximum mass of neutron star: those in the constraints have smaller maximum mass, and those above the constraints have larger maximum mass. The results of bsHLS-L and bsHLS-H are both above the constraints, and bsHLS-L is even above the chiral nuclear force results. One reason for this is that the HIC flow-data constraints are not included in our fitting process, and possible ways to fix the discrepancy will be discussed later in this section.

Before the kink of the incompressibility at $\sim 2n_0$ (also the kink of pressure) in Fig. 1, the pressure of bsHLS is smaller than those of all the compared Walecka-type models, and such kink behavior is not excluded by the constraints, which offers the opportunity for a compact but heavy NS.

The key difference lies in β' for bsHLS-H and bsHLS-L, which is connected to the existence of the pseudo-conformal structure at high densities [40]. The β' of bsHLS-H aligns with the constraints of the pseudo-conformal limit, whereas the β' of bsHLS-L does not. This highlights the impact of scale symmetry patterns on NS M-R relations.

Moreover, because σ is nonlinearly coupled with other mesons (see Eq. (8)) through a conformal compensator, its density dependence shows a kink behavior that is not observed in Walecka-type models [70]. As a result, the order parameter $\langle\chi\rangle^*$, calculated based on bsHLS, does not approach zero throughout the density regions, which is necessary for the (pseudo-)conformal limits of QCD at high densities [35, 40, 89]. Considering the derivation of bsHLS to HIC flow-data analysis and to recover the expected behavior of $\langle\chi\rangle^*$, a possible approach is to couple an additional factor to $g_{\omega NN}$ to obtain the effective coupling $\tilde{g}_{\omega NN} = g_{\omega NN}/(1+R\frac{\rho_p+\rho_n}{n_0})$ [70, 90].

As shown in Table 5, the NM properties can be reproduced with the parameter set bsHLS-HS: $M_\sigma = 2.25\times 10^5$ MeV^2, $\beta' = 1.14$, $g_{\omega NN} = 11.5$, $g_{\rho NN} = 4.27, g^{SSB}_{\omega NN} = 8.70$, $g^{SSB}_{\rho NN} = 4.85$, $r = 0.20$, and $R = 0.02$. Moreover, as shown in Fig. 6, the M-R relations for PNM are roughly

Table 5. Quantities of nuclear matter with additional suppressions of $\tilde{g}_{\omega NN}$. The definitions and constraints are the same as in Table 1.

	n_0	e_0	K_0	$E_{\rm sym}(n_c)$	$E_{\rm sym}(n_0)$	$E_{\rm sym}(2n_0)$	$L(n_c)$	$L(n_0)$	J_0
bsHLS-HS	0.159	-16.0	259	21.6	30.3	52.9	55.4	74.5	-720

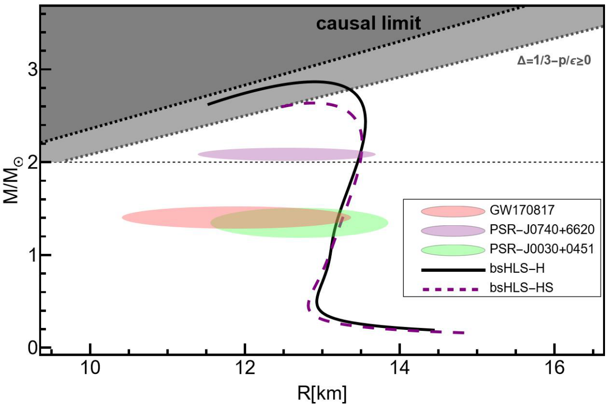

Fig. 6. (color online) NS M-R relation results with/without $g_{\omega NN}$ suppression.

consistent with observational constraints, but there is a decrease in $M_{\rm max}$ compared to bsHLS-H, which makes the M-R relation fall within the positive trace anomaly region.

To understand the discrepancies in the M-R relations, the incompressibilities and symmetry energies are also calculated for bsHLS-H and bsHLS-HS, as shown in Fig. 7.

It can be seen that the symmetry energy remains almost the same in both cases. However, the incompressibility of bsHLS-HS is much softer than that of bsHLS-H at high densities, leading to a decrease in $M_{\rm max}$. This gives us a hint to find a model compatible with the HIC SNM pressure constraint by introducing a suppression factor, as shown in Fig. 8, which also provides the rationality from the phenomenological side to add such suppression at high densities.

At low or intermediate densities, the incompressibilities of both cases are similar, which results in the M-R relations being comparable in the region of NS constraints.

Additionally, the NM properties are investigated with B-R scaling turned off. We find that with the parameter set of bsHLS-N ($M_\sigma = 1.11\times10^5$ MeV^2, $\beta' = 1.10$, $g_{\omega NN} = -11.0$, $g_{\rho NN} = 4.17$, $g_{\omega NN}^{SSB} = -192$, and $g_{\rho NN}^{SSB} = 4.85$), the NM properties can still be reproduced (*e.g.*, $n_0 = 0.16$ fm^{-3}, $e_0 = -16.0$ MeV, $K_0 = 241$ MeV, $E_{\rm sym}(n_0) = 29.3$ MeV). However, this approach results in a much softer scale symmetry parameter $\langle\chi\rangle^*$ flow compared to the cases with B-R scaling. As a result, the M-R relation becomes unnatural and deviates from the constraints, as shown in Fig. 9.

All these findings, including the necessity of introducing $\tilde{g}_{\omega NN}$ suppression and B-R scaling, signify the importance of properly parameterizing the scale symmetry

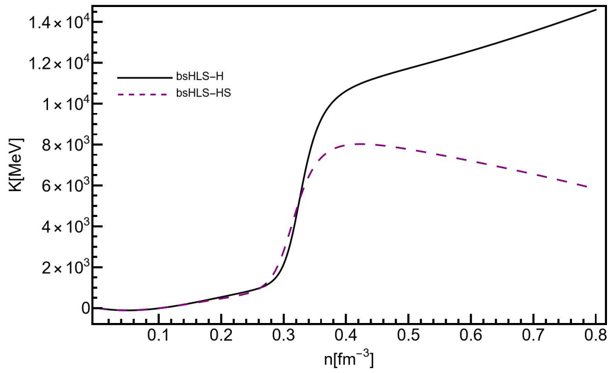

(a) Incompressibilities as a function of density in SNM.

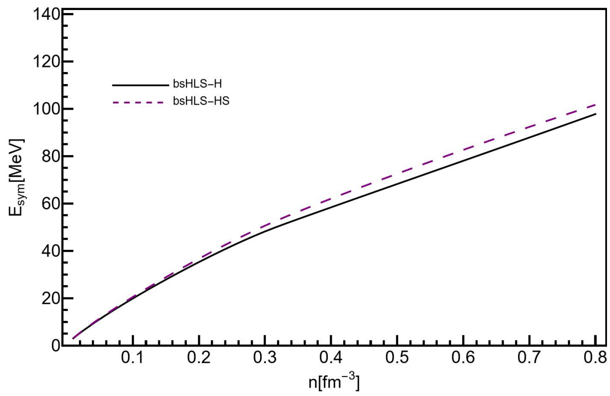

(b) Symmetry energies as a function of density.

Fig. 7. (color online) NM property results with/without $g_{\omega NN}$ suppression.

in densities. This reminds us of past work on the quenching factors of g_A, which affect the β decay of neutrons in dense environments (see Ref. [38] for details). From the comparison among the various cases discussed above, valuable lessons about NS and NM properties have been learned, providing guidance on hadron interaction parameterization to describe dense NM. Because the differences between bsHLS and Walecka-type models in our analysis are at intermediate density regions, not far from n_0, it is expected that examining bsHLS in dense systems will be promising in future experiments.

IV. CONCLUSION AND DISCUSSION

In this study, the bsHLS, constructed based on the philosophy of χEFT with HLS and a possible IR fixed point of QCD at low energies, was applied to dense environments using the RMF approximation, with free parameters fixed by pinning the nuclei structure data around

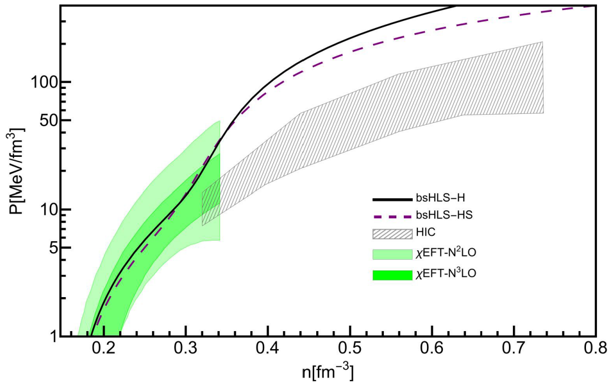

Fig. 8. (color online) Pressure as a function of density for SNM with bsHLS model.

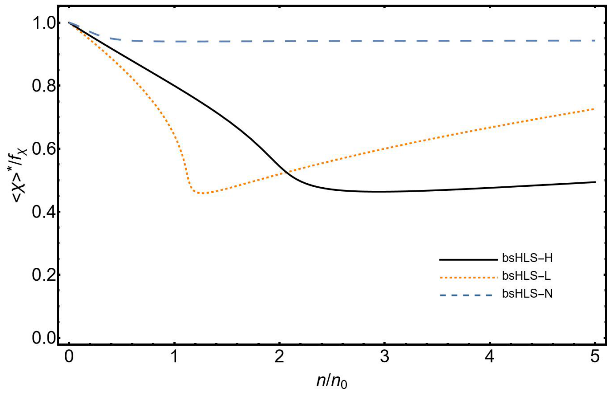

(a) $\langle\chi\rangle^*/f_\chi$ as a function of density.

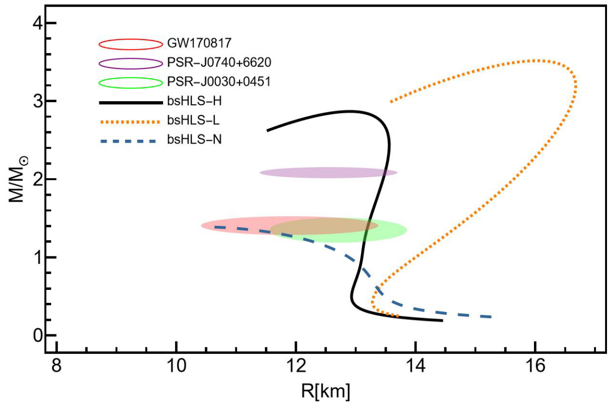

(b) MR relation of NS.

Fig. 9. (color online) $\langle\chi\rangle^*/f_\chi$ in pure neutron matter and NS M-R relation results with/without B-R scaling.

n_0. The NM properties and NS M-R relations can be well reproduced, closely matching empirical values in the bsHLS-H case.

Without introducing many freedoms, such as the δ meson, and with operators organized to respect chiral and scale symmetry considerations and expanded by chiral-scale orders, the bsHLS can provide a reasonable behavior of NM properties from subsaturation to intermediate densities, *e.g.*, $K(n)$ and $E_{\rm sym}(n)$, compared to Walecka-type models. Moreover, the NS M-R relations are sensitive to NM properties at these density regions, making bsHLS outperform Walecka-type models in describing a wider range of densities. More specifically, the kink behavior of the σ field in bsHLS at intermediate densities allows the $M_{\rm max}$ to reach nearly $3\,M_\odot$ for PNM, while other NS observational constraints are still satisfied.

However, the above discussions are all based on analysis where parameter sets are fitted to the nuclear matter properties around saturation density, and then EOSs are extended to neutron star matter. In principle, the parameter sets may describe the neutron star matter better if they include the neutron star observations in the fitting process. Further study on this topic will be improved by a more systematic fitting procedure, as discussed in Ref. [50], which will help to refine the parameter sets and enhance the predictive power of the model.

Besides, the behaviors of symmetry patterns in dense environments are also found to be pivotal to macroscopic phenomena. If there is no restoration point of scale symmetry at certain densities, such as the β' value of bsHLS-L, the NS M-R relations will fall outside observational constraints. The $M_{\rm max}$ of predicted NSs is influenced by the behavior of the order parameter of scale symmetry, $\langle\chi\rangle^*$.

Furthermore, the study of the flow of $\langle\chi\rangle^*$ with densities suggests the necessity of introducing an additional suppression factor for $\tilde{g}_{\omega NN}$ to recover the scale symmetry, and it could be an interesting problem for further investigation. As a good starting point, recovering the expected scale symmetry behavior has been shown to be a possible way to heal the discrepancy with the HIC flow-data analysis. A more systematic study on the analysis of HIC flow data with the bsHLS can be conducted in the future via: I. including the potential induced by our approach, where the σ meson is introduced as a exponential field χ in the transport model [91], II. including the HIC flow-data constraints in our fitting process in addition to the NM properties around saturation density, and III. introducing the additional suppression from a more fundamental consideration of QCD.

In summary, introducing bsHLS to NM studies is a promising approach due to its close relation to QCD symmetry patterns and the effective potentials organized by chiral-scale orders, which have already proven successful in describing scattering experiments under vacuum. The relationship between microscopic symmetries and macroscopic phenomena found in this work is also a valuable topic to be further studied.

ACKNOWLEDGMENTS

We would like to thank Yi-Zhong Fan for his valuable comments.

References

[1] B. D. Serot and J. D. Walecka, Adv. Nucl. Phys. **16**, 1 (1986)
[2] G. E. Brown and M. Rho, Phys. Rept. **363**, 85 (2002), arXiv: hep-ph/0103102
[3] K. Fukushima and T. Hatsuda, Rept. Prog. Phys. **74**, 014001 (2011), arXiv: 1005.4814[hep-ph]
[4] J. M. Lattimer and M. Prakash, The Equation of State of Hot, Phys. Rept. **621**, 127 (2016), arXiv: 1512.07820[astro-ph.SR]
[5] G. Baym, T. Hatsuda, T. Kojo *et al.*, Rept. Prog. Phys. **81**, 056902 (2018), arXiv: 1707.04966[astro-ph.HE]
[6] Y.-L. Ma and M. Rho, Prog. Part. Nucl. Phys. **113**, 103791 (2020a), arXiv: 1909.05889[nucl-th]
[7] L. Brandes and W. Weise, Symmetry **16**, 111 (2024), arXiv: 2312.11937[nucl-th]
[8] K. Holinde and R. Machleidt, Momentum Space Obep, Nucl. Phys. A **247**, 495 (1975)
[9] K. Erkelenz, Phys. Rept. **13**, 191 (1974)
[10] M. M. Nagels, T. A. Rijken, and J. J. de Swart, Phys. Rev. D **17**, 768 (1978)
[11] R. Machleidt, Adv. Nucl. Phys. **19**, 189 (1989)
[12] J. D. Walecka, Annals Phys. **83**, 491 (1974)
[13] R. B. Wiringa, V. Fiks, and A. Fabrocini, Phys. Rev. C **38**, 1010 (1988)
[14] B. Gao, T. Minamikawa, T. Kojo *et al.*, Phys. Rev. C **106**, 065205 (2022), arXiv: 2207.05970[nucl-th]
[15] B. Gao and M. Harada, Phys. Rev. D **111**, 016024 (2025), arXiv: 2410.16649[nucl-th]
[16] S. Weinberg, Physica A **96**, 327 (1979)
[17] S. Weinberg, Nucl. Phys. B **363**, 3 (1991)
[18] J. Gasser and H. Leutwyler, Annals Phys. **158**, 142 (1984)
[19] S. Scherer, Adv. Nucl. Phys. **27**, 277 (2003), arXiv: hep-ph/0210398
[20] J. Bijnens, G. Colangelo, G. Ecker *et al.*, Phys. Lett. B **374**, 210 (1996), arXiv: hep-ph/9511397
[21] M. R. Schindler and D. R. Phillips, Bayesian Methods for Parameter Estimation in Effective Field Theories, Annals Phys. **324**, 682 (2009), [Erratum: Annals Phys. 324, 2051–2055 (2009)]., arXiv: 0808.3643
[22] S. Wesolowski, N. Klco, R. J. Furnstahl *et al.*, J. Phys. G **43**, 074001 (2016), arXiv: 1511.03618[nucl-th]
[23] T. N. Truong, Phys. Rev. Lett. **61**, 2526 (1988)
[24] J. A. Oller, E. Oset, and J. R. Pelaez, Phys. Rev. Lett. **80**, 3452 (1998), arXiv: hep-ph/9803242
[25] M. Bando, T. Kugo, S. Uehara *et al.*, Phys. Rev. Lett. **54**, 1215 (1985)
[26] M. Bando, T. Kugo, and K. Yamawaki, Phys. Rept. **164**, 217 (1988)
[27] M. Harada and K. Yamawaki, Phys. Rept. **381**, 1 (2003), arXiv: hep-ph/0302103
[28] R. J. Crewther and L. C. Tunstall, Phys. Rev. D **91**, 034016 (2015), arXiv: 1312.3319[hep-ph]
[29] O. Catà, R. J. Crewther, and L. C. Tunstall, Phys. Rev. D **100**, 095007 (2019), arXiv: 1803.08513[hep-ph]
[30] H. K. Lee, W.-G. Paeng, and M. Rho, Phys. Rev. D **92**, 125033 (2015), arXiv: 1504.00908[nucl-th]
[31] Y.-L. Li, Y.-L. Ma, and M. Rho, Phys. Rev. D **95**, 114011 (2017), arXiv: 1609.07014[hep-ph]
[32] S. K. Bogner, T. T. S. Kuo, and A. Schwenk, Phys. Rept. **386**, 1 (2003), arXiv: nucl-th/0305035
[33] J. W. Holt, G. E. Brown, J. D. Hol *et al.*, Nucl. Phys. A **785**, 322 (2007), arXiv: nucl-th/0610069
[34] Y.-L. Ma and M. Rho, Phys. Rev. D **99**, 014034 (2019a), arXiv: 1810.06062[nucl-th]
[35] Y.-L. Ma and M. Rho, Phys. Rev. D **100**, 114003 (2019b), arXiv: 1811.07071[nucl-th]
[36] Y.-L. Ma, H. K. Lee, W.-G. Paeng *et al.*, Sci. China Phys. Mech. Astron. **62**, 112011 (2019), arXiv: 1804.00305[nucl-th]
[37] D. Lubos *et al.*, Phys. Rev. Lett. **122**, 222502 (2019)
[38] Y.-L. Ma and M. Rho, Phys. Rev. Lett. **125**, 142501 (2020b), arXiv: 2002.03310[nucl-th]
[39] Y.-L. Ma and M. Rho, Scale-chiral symmetry, Phys. Rev. D **97**, 094017 (2018), arXiv: 1612.04079[nucl-th]
[40] L.-Q. Shao and Y.-L. Ma, Phys. Rev. D **106**, 014014 (2022), arXiv: 2202.09957[nucl-th]
[41] H.-J. Lee, B.-Y. Park, M. Rho, and V. Vento, Nucl. Phys. A **726**, 69 (2003), arXiv: hep-ph/0304066
[42] B.-Y. Park, M. Rho, and V. Vento, Nucl. Phys. A **807**, 28 (2008), arXiv: 0801.1374[hep-ph]
[43] B. P. Abbott *et al.* (LIGO Scientific, Virgo), Phys. Rev. Lett. **121**, 161101 (2018), arXiv: 1805.11581[gr-qc]
[44] B. T. Reed, F. J. Fattoyev, C. J. Horowitz *et al.*, Phys. Rev. Lett. **126**, 172503 (2021), arXiv: 2101.03193[nucl-th]
[45] F. Li, B.-J. Cai, Y. Zhou *et al.*, Astrophys. J. **929**, 183 (2022), arXiv: 2202.08705[nucl-th]
[46] Y. Ma and Y.-L. Ma, Phys. Rev. D **109**, 074022 (2024), arXiv: 2311.07899[nucl-th]
[47] B. P. Abbott *et al.* (LIGO Scientific, Virgo), Phys. Rev. X **9**, 011001 (2019), arXiv: 1805.11579[gr-qc]
[48] M. C. Miller *et al.*, Astrophys. J. Lett. **918**, L28 (2021), arXiv: 2105.06979[astro-ph.HE]
[49] T. E. Riley *et al.*, Astrophys. J. Lett. **918**, L27 (2021), arXiv: 2105.06980[astro-ph.HE]
[50] L.-J. Guo, J.-Y. Xiong, Y. Ma *et al.*, Astrophys. J. **965**, 47 (2024), arXiv: 2309.11227[nucl-th]
[51] S. Shirke, R. Maiti, and D. Chatterjee, PSR J0614-3329: A NICER case for Strange Quark Stars (2025), arXiv: 2508.02652
[52] F. J. Fattoyev, J. Piekarewicz, and C. J. Horowitz, Phys. Rev. Lett. **120**, 172702 (2018), arXiv: 1711.06615[nucl-th]
[53] Y.-L. Li and Y.-L. Ma, Derivation of Brown-Rho scaling from scale-chiral perturbation theory, arXiv: 1710.02839
[54] G. E. Brown and M. Rho, Phys. Rev. Lett. **66**, 2720 (1991)
[55] P. Kienle and T. Yamazaki, Pions in nuclei, Prog. Part. Nucl. Phys. **52**, 85 (2004)
[56] R. L. Workman *et al.* (Particle Data Group), PTEP **2022**, 083C01 (2022)
[57] A. Sedrakian, J.-J. Li, and F. Weber, Prog. Part. Nucl. Phys. **131**, 104041 (2023), arXiv: 2212.01086[nucl-th]
[58] M. Dutra, O. Lourenco, J. S. Sa Martins *et al.*, Phys. Rev. C **85**, 035201 (2012), arXiv: 1202.3902[nucl-th]
[59] L.-W. Chen, Phys. Rev. C **83**, 044308 (2011), arXiv: 1101.5217[nucl-th]
[60] M. Liu, N. Wang, Z.-X. Li, and F.-S. Zhang, Phys. Rev. C **82**, 064306 (2010), arXiv: 1011.3865[nucl-th]
[61] J. M. Lattimer and Y. Lim, Astrophys. J. **771**, 51 (2013), arXiv: 1203.4286[nucl-th]
[62] B.-A. Li, P. G. Krastev, D.-H. Wen *et al.*, Eur. Phys. J. A **55**, 117 (2019), arXiv: 1905.13175[nucl-th]
[63] Z. Zhang and L.-W. Chen, Phys. Rev. C **90**, 064317 (2014), arXiv: 1407.8054[nucl-th]
[64] W.-J. Xie and B.-A. Li, Astrophys. J. **883**, 174 (2019), arXiv: 1907.10741[astro-ph.HE]

[65] M. Dutra, O. Loureno, S. S. Avancini *et al.*, Phys. Rev. C **90**, 055203 (2014), arXiv: 1405.3633[nucl-th]

[66] G. A. Lalazissis, J. Konig, and P. Ring, Phys. Rev. C **55**, 540 (1997), arXiv: nucl-th/9607039

[67] Y. Sugahara and H. Toki, Nucl. Phys. A **579**, 557 (1994)

[68] B. K. Agrawal, Phys. Rev. C **81**, 034323 (2010), arXiv: 1003.3295[nucl-th]

[69] S. K. Dhiman, R. Kumar, and B. K. Agrawal, Phys. Rev. C **76**, 045801 (2007), arXiv: 0709.4081[nucl-th]

[70] L.-Q. Zhang, Y. Ma, and Y.-L. Ma, Peak of sound velocity, scale symmetry and nuclear force in baryonic matter (2024), arXiv: 2410.04142

[71] T. E. Riley *et al.*, Astrophys. J. Lett. **887**, L21 (2019), arXiv: 1912.05702[astro-ph.HE]

[72] Y. Fujimoto, K. Fukushima, L. D. McLerran *et al.*, Phys. Rev. Lett. **129**, 252702 (2022), arXiv: 2207.06753[nucl-th]

[73] J. R. Oppenheimer and G. M. Volkoff, Phys. Rev. **55**, 374 (1939)

[74] R. C. Tolman, Phys. Rev. **55**, 364 (1939)

[75] G. Baym, C. Pethick, and P. Sutherland, Astrophys. J. **170**, 299 (1971)

[76] W. D. Arnett and R. L. Bowers, Astrophys. J. Suppl. **33**, 415 (1977)

[77] S. Postnikov, M. Prakash, and J. M. Lattimer, Phys. Rev. D **82**, 024016 (2010), arXiv: 1004.5098[astro-ph.SR]

[78] A. Deur, S. J. Brodsky, and G. F. de Teramond, Phys. Lett. B **750**, 528 (2015), arXiv: 1409.5488[hep-ph]

[79] F. Özel, P. Freire, Ann. Rev. Astron. Astrophys. **54**, 401 (2016), arXiv: 1603.02698[astro-ph.HE]

[80] Y.-Z. Fan, M.-Z. Han, J.-L. Jiang *et al.*, Phys. Rev. D **109**, 043052 (2024), arXiv: 2309.12644[astro-ph.HE]

[81] C. J. Horowitz and B. D. Serot, Nucl. Phys. A **368**, 503 (1981)

[82] C. D. Bailyn, R. K. Jain, P. Coppi *et al.*, Astrophys. J. **499**, 367 (1998), arXiv: astro-ph/9708032

[83] W. M. Farr, N. Sravan, A. Cantrell *et al.*, Astrophys. J. **741**, 103 (2011), arXiv: 1011.1459[astro-ph.GA]

[84] R. Abbott *et al.* (LIGO Scientific, Virgo), Astrophys. J. Lett. **896**, L44 (2020), arXiv: 2006.12611[astro-ph.HE]

[85] S. O. Backman, G. E. Brown, and J. A. Niskanen, Phys. Rept. **124**, 1 (1985)

[86] C. Drischler, J. W. Holt, and C. Wellenhofer, Ann. Rev. Nucl. Part. Sci. **71**, 403 (2021), arXiv: 2101.01709[nucl-th]

[87] P. Danielewicz, R. Lacey, and W. G. Lynch, Science **298**, 1592 (2002), arXiv: nucl-th/0208016

[88] S. Huth *et al.*, Nature **606**, 276 (2022), arXiv: 2107.06229[nucl-th]

[89] S. Borsanyi, Z. Fodor, C. Hoelbling *et al.*, Phys. Lett. B **730**, 99 (2014), arXiv: 1309.5258[hep-lat]

[90] W.-G. Paeng, H. K. Lee, M. Rho *et al.*, Phys. Rev. D **88**, 105019 (2013), arXiv: 1303.2898[nucl-th]

[91] A. Sorensen *et al.*, Prog. Part. Nucl. Phys. **134**, 104080 (2024), arXiv: 2301.13253[nucl-th]